AMERICAN ACADEMY OF OPHTHALMOLOGY®

Eccentric Pathology in Keratoconus Exhibits Stiffer Biomechanical Response than Central Pathology

Cameron D. Bruner, BS, MD,[1] *Ashraf M. Mahmoud, BS,*[1,2] *Cynthia J. Roberts, PhD*[1,2]

Purpose: To investigate the difference in biomechanical response metrics between central and eccentric pathology and compare axial vs. tangential curvature, as well as zonal vs. single-point values.

Design: Prospective, observational, cross-sectional study.

Participants: The study included 67 eyes of 41 subjects diagnosed with keratoconus (KCN).

Methods: Pentacam tomography and Corvis ST examinations were acquired, and disease severity was defined by maximum curvature, comparing single point of maximum anterior axial curvature (Kmax) vs. magnitude of surrounding 2 mm zonal value (ZKmax) on axial maps, vs. magnitude of steepest 2 mm zone on axial (CSpot_Axi) and tangential (CSpot_Tan) maps located by Cone Location and Magnitude Index (CLMI). Distance between the corneal center and Kmax (Kmax_dist) was compared to radial distance with CLMI (CRad_Axi and CRad_Tan). Single-point Kmax, ZKmax, and CLMI-derived zones were compared with biomechanical metrics via regression analyses, including stiffness parameter at first applanation (SP-A1), deformation amplitude ratio at 2 mm (DA Ratio), integrated inverse radius (IIR), and stress–strain index (SSI). Measurements were analyzed using paired *t* tests, with *t* tests between central and eccentric disease, and a significance threshold, $P < 0.05$.

Main Outcome Measures: Maximum curvature using axial vs. tangential curvature, zonal vs. single-point curvature, and corneal stiffness metrics compared with cone location.

Results: Significantly greater central pathology was found using tangential (58 central and 9 eccentric) vs. axial curvature (28 central and 39 eccentric). ZKmax was significantly different than CSpot_Axi and CSpot_Tan ($P < 0.0001$). CRad_Axi (1.53 ± 0.41 mm) was significantly greater ($P < 0.001$) than Kmax_dist (1.33 ± 0.56 mm) and CRad_Tan (0.99 ± 0.34 mm). Kmax (56.09 ± 8.99 diopter [D]) was significantly greater than ZKmax (51.81 ± 7.50 D). Regressions for ZKmax, CSpot_Axi, and CSpot_Tan were significantly negative to SP-A1, stiffness parameter at highest concavity, and SSI, whereas significantly positive to DA Ratio and IIR. Regressions for Kmax_dist, CRad_Axi, and CRad_Tan had significantly positive relationships to SSI and significantly negative relationships to DA Ratio and IIR.

Conclusions: Central pathology has greater frequency with tangential than axial curvature. Corneal stiffness increases as the distance of the cone from the center increases, consistent with the focal nature of KCN. Central stiffness decreases as cone curvature (disease severity) increases. Recommendation is to use zonal values with tangential curvature to evaluate the location of the greatest curvature and changes in curvature over time.

Financial Disclosure(s): Proprietary or commercial disclosure may be found in the Footnotes and Disclosures at the end of this article. *Ophthalmology Science 2025;5:100682 © 2025 by the American Academy of Ophthalmology. This is an open access article under the CC BY-NC-ND license (http://creativecommons.org/licenses/by-nc-nd/4.0/).*

Keratoconus (KCN) is a bilateral progressive corneal ectasia that can lead to visually debilitating corneal changes. It begins primarily during adolescence and affects approximately 0.138% of the world's population, although the distribution is not uniform with the greatest reported prevalence in Saudi Arabia at 4.79%.[1,2] Although the exact etiology of the condition is unknown, it has been associated with a number of conditions such as eye rubbing, oxidative stress, genetic predispositions, and atopy.[3–5] Keratoconus is characterized by progressive corneal thinning and subsequent focally increased curvature, leading to refractive changes such as worsening myopia and irregular astigmatism.[6] More advanced cases can lead to corneal scarring or progressive thinning predisposing to acute hydrops.[7]

Many of the morphologic changes observed in KCN are likely secondary to mechanical weakness and a reduced ability to resist deformation under the stress of intraocular pressure (IOP).[8] However, rather than a global weakening, KCN shows a predilection for focal weakening, which drives the subsequent decreasing thickness and increasing curvature.[9–11] Studies have shown a lower modulus is associated with the keratoconic cone relative to the surrounding tissue, using Brillouin microscopy.[10,11] The pathology underlying the area of the cone shows a tendency for thinning and steepening whereas the

https://doi.org/10.1016/j.xops.2024.100682
ISSN 2666-9145/25

remainder of the cornea tends toward flattening, generating asymmetry. This focal weakening leads to a cycle of corneal decompensation characterized by progressive thinning and increasing focal curvature.[9] Meek et al[12] showed that the normal lamellar organization of the cornea was disrupted in KCN near the pathology, also consistent with focal weakening. Thus, the morphologic changes observed in KCN are likely to be secondary to focal biomechanical abnormalities in the diseased cornea.[9–13] Roberts and Dupps[9] proposed that by assessing biomechanical asymmetry, KCN and subclinical KCN might be detected before the onset of thinning and steepening.

Currently, biomechanical devices such as the Corvis ST are unable to identify asymmetry or focal changes in the cornea. This limitation stems from their design to record corneal deformation response to central air puff loading, therefore producing metrics of global corneal response.[14–17] Promisingly, the addition of tomographic parameters to account for location-specific changes in thickness and curvature has shown to be even more effective in the detection of KCN and subclinical KCN than biomechanical measurements alone.[15,18] Tomography allows for the assessment of asymmetry that biomechanical response with current devices cannot. However, it is also possible that central pathology may generate different biomechanical response parameters than eccentric pathology due to the potential location away from the center. It is, therefore, the intention of this study to investigate the relationship between measured corneal stiffness with central air puff loading in keratoconic subjects as a function of disease severity and distance of the keratoconic cone from the corneal center. Because of the proposed focal nature of the pathologic changes in KCN, we propose that corneal stiffness under central loading will be lowest with central pathology and will increase according to the further eccentric the keratoconic cone is located. It is also proposed to compare axial curvature with tangential curvature for determining the location of the pathology.

Methods

This prospective cohort study was conducted at the Havener Eye Institute of The Ohio State University Department of Ophthalmology and Visual Sciences in Columbus, Ohio. Institutional review board approval was obtained before the commencement of the study, which adhered to the Declaration of Helsinki. Informed consent was obtained from all participants before the initiation of data collection.

Participants were recruited from The Ohio State University Department of Ophthalmology and Visual Sciences, referred from optometrists in the College of Optometry at The Ohio State University, and referred from community ophthalmologists/optometrists. Inclusion criteria were the following: a clear cornea; the ability and willingness to comply with the study protocol; the age of $\geq$18 years; a diagnosis of KCN with clinical signs, including $\geq$1 of reduced corneal thickness, steepening, Fleischer ring, Vogt striae, or scissoring. Exclusion criteria included the following: nonintact epithelium; pregnancy; $<$12 weeks postpartum or from the cessation of breastfeeding; nystagmus; previous ocular surgery, except cataract extraction $>$3 months before date of enrollment; comorbidities including diabetes; systemic disease that causes defects in collagen, such as Marfan's syndrome; and glaucoma or medications that affect biomechanics, such as topical prostaglandin analogs.

Pentacam HR tomography and Corvis ST (Oculus) biomechanical response metrics were prospectively acquired. Multiple measurements were taken to obtain at least 3 evaluable examinations for each eye. Topical lubricating eye drops were used as needed to ensure ocular comfort and promote the acquisition of high-quality images and measurements. The location and magnitude of the single point of maximum anterior axial curvature (Kmax) were recorded along with x and y coordinates (see Fig 1A) from the 4 Maps Selectable display to be used in the determination of zonal Kmax (ZKmax), which was not included in the export and must be manually extracted. ZKmax was defined as the magnitude of a 2.0 mm diameter circular zone centered around Kmax and was ultimately generated in the Corneal Power Distribution display by entering the coordinates from the first display and defining the zone size (see Fig 1B). The average corneal curvature of ZKmax was obtained from this second display and the distance between the corneal center and Kmax (Kmax_dist) was then calculated independently using the distance formula. If Kmax_dist was $>$2.6 mm, the threshold used by the Pentacam, then the value of 2.6 mm was assigned. Therefore, any eye with Kmax $\geq$2.6 mm was excluded from analysis for comparison with values obtained using custom software without a threshold. These same maps were then exported, and custom software was used to generate Cone Location and Magnitude Index (CLMI) parameters, described elsewhere.[6] Briefly, a search algorithm was used to identify the maximum 2 mm circular region (CSpot) of maximum axial and tangential curvature, CSpot_Axi and CSpot_Tan, respectively.[6] The radial distances from the map center to the center of CSpot_Axi and CSpot_Tan were also calculated: CRad_Axi and CRad_Tan, respectively. Multiple Pentacam measurements for each eye were then averaged to obtain mean data for statistical analysis. Additionally, the location of the cone was categorized as central if the center of CSpot was located within the central 3 mm diameter corneal zone inclusive, and eccentric if the center of CSpot was outside of this zone.

Corvis ST, a device that is United States Food and Drug Administration-approved for noncontact tonometry and pachymetry, uses an ultra-highspeed Scheimpflug camera to capture a series of 140 images of the cornea deforming under an air puff with consistent spatial and temporal profile.[19,20] These images provide direct information on the shape of the deformation response in an 8 mm window of the horizontal corneal meridian. Processing with the research software (version 1.6r2187) provides multiple biomechanical response parameters including stiffness parameter at first applanation (SP-A1), stiffness parameter at highest concavity (SP-HC), deformation amplitude ratio at 2 mm (DA Ratio), integrated inverse radius (IIR), and corneal stress−strain index (SSI). Corvis ST measurements for each eye were then averaged to obtain mean measurements for each recorded parameter.

Data between central and eccentric groups were compared using *t* tests, and measurements within each group were compared using paired *t* tests. Single-point Kmax, ZKmax, and CLMI-derived zones were compared via univariate regression analyses with biomechanical metrics to evaluate the severity of disease by the relationship between maximum curvature and stiffness. The SP-A1, SSI, and SP-HC, all increase with increasing stiffness, whereas DA Ratio and IIR, both decrease with increasing stiffness. The location of the cone by Kmax_dist, CRad_Axi, and CRad_Tan was compared with biomechanical metrics via regression. Neither

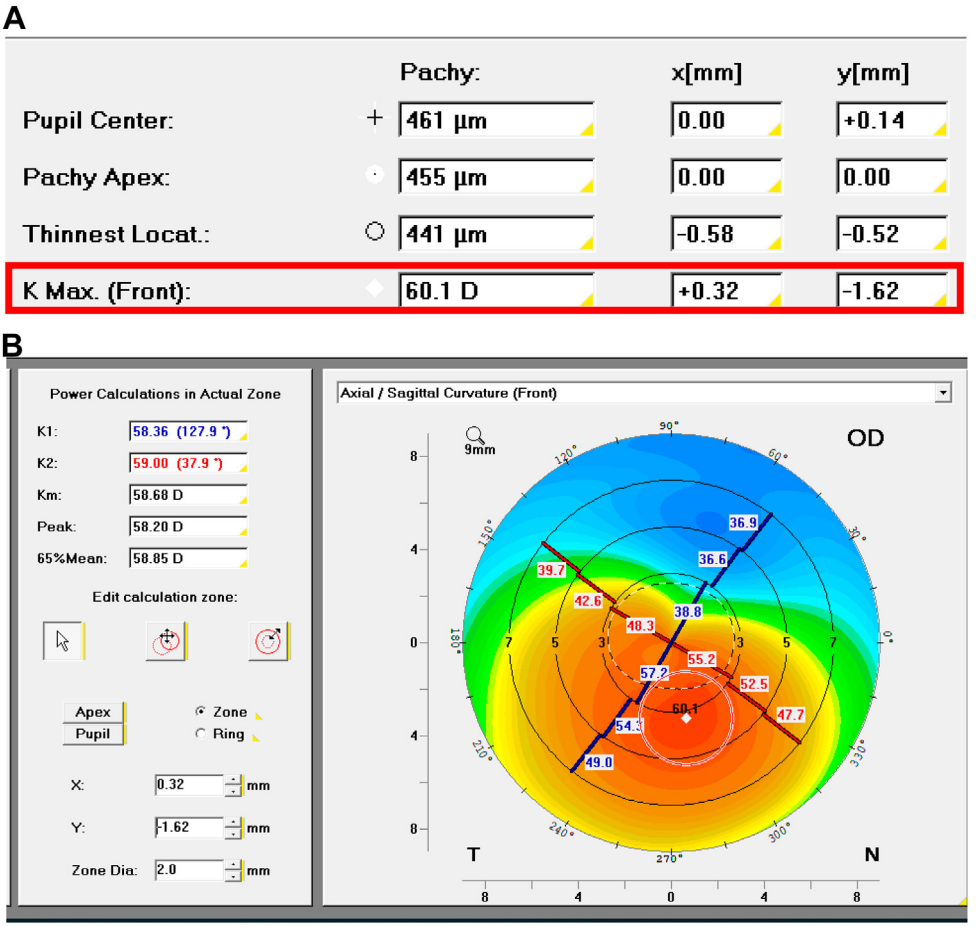

Figure 1. A, Pentacam single point of maximum anterior axial curvature (Kmax) magnitude and coordinates from the 4 Maps Selectable display. **B,** Pentacam axial corneal curvature map with 2.0 mm zonal Kmax (ZKmax) centered on the location of single-point Kmax from the Corneal Power Distribution display.

age nor IOP would influence the regression of location because the entire cornea would be biomechanically impacted. However, central corneal thickness (CCT) could potentially have an influence because it would be thicker centrally with an eccentric cone. Therefore, univariate regression was performed if there were no differences in CCT between the central and eccentric groups. Multiple regression was performed if significant differences were found. Statistical analyses were performed in SAS with a significance threshold of $P < 0.05$.

Results

A total of 67 eyes of 41 subjects were enrolled with a diagnosis of KCN, and 44% were female. There were 6 KCN eyes with Kmax greater than or equal to 2.6 mm; hence, 61 eyes were ultimately analyzed for comparisons that included Kmax_dist. The age, biomechanically corrected IOP, and CCT, as well as tomographic and biomechanical parameters, are summarized in Table 1. Single point Kmax was found to be significantly greater than zonal ZKmax. CSpot_Axi and CSpot_Tan were found to have significantly greater average magnitudes than ZKmax ($P < 0.001$). In terms of distance from the center, CRad_Axi was found to be significantly greater than Kmax_dist and CRad_Tan ($P < 0.001$). CRad_Axi and CRad_Tan were significantly different as well ($P < 0.0001$) with CRad_Axi having an average of 0.54 ± 0.13 mm greater distance from the corneal center. There was a greater number of central cones defined by tangential curvature (58 central and 9 eccentric) than by axial curvature (28 central and 39 eccentric). Cone location percentages are summarized in Table 2, along with age, biomechanically corrected IOP, CCT, as well as biomechanical and tomographic parameters comparisons between the central and eccentric cones. Most parameters are significantly different between central and eccentric cones, with the exception of CSpot_Tan, which can be interpreted as maximum cone curvature to indicate severity. Therefore, both central and eccentric cones have similar severity based on curvature, as well as age, and biomechanically corrected IOP. Using the axial algorithm, there was no difference in CCT between central and eccentric cones. However, using the tangential algorithm, eccentric cones had significantly greater CCT. Examples of central and eccentric cones using both axial and tangential algorithms are shown in Figure 2A to C, illustrating not only the difference between eccentric (radial distance >1.5 mm) and central cones (radial

Table 1. Summary of Biomechanical and Tomographic Parameters in Keratoconus

Variable (Units)	Mean ± Std Dev
Age (yrs)	35 ± 13
bIOP (mmHg)	13.1 ± 2.9
Central corneal thickness (μ)	486 ± 49
SP-A1 (mmHg/mm)	67.6 ± 25.1
SP-HC (mmHg/mm)	8.07 ± 3.43
DA Ratio (unitless)	5.96 ± 1.87
IIR (1/mm)	11.60 ± 3.37
SSI (unitless)	0.83 ± 0.17
Kmax (D)	56.09 ± 8.99*,†
ZKmax (D)	51.81 ± 7.50*,†
CSpot_Axi (D)	54.48 ± 8.33*
CSpot_Tan (D)	53.67 ± 7.73†
Kmax_dist (mm)	1.33 ± 0.56‡
CRad_Axi (mm)	1.53 ± 0.41‡
CRad_Tan (mm)	0.99 ± 0.34‡

Of the curvature values in D, only CSpot_Axi and CSpot_Tan are not significantly different from each other.
bIOP = biomechanically corrected intraocular pressure; CRad_Axi = distance from the corneal center to CSpot_Axi; CRad_Tan = distance from the corneal center to CSpot_Tan; CSpot_Axi = CLMI-derived steepest 2.0 mm diameter zone on the axial map; CSpot_Tan = CLMI-derived steepest 2.0 mm diameter zone on the tangential map; D = diopter; DA Ratio = deformation amplitude ratio at 2 mm; IIR = integrated inverse radius; Kmax = single point of maximum anterior axial curvature; Kmax_dist = distance between the corneal center and Kmax; SP-A1= stiffness parameter at first applanation; SP-HC = stiffness parameter at highest concavity; SSI = corneal stress–strain index; ZKmax = 2.0 mm diameter zone centered around Kmax.
*Indicates significant difference between all 3 values: CSpot_Axi, Kmax, and ZKmax; $P < 0.0001$.
†Indicates significant differences between all 3 values: CSpot_Tan, Kmax, and ZKmax; $P < 0.0001$.
‡Indicates significant difference between all 3 distances, $P < 0.001$.

distance ≤1.5 mm) but also that axial is a running average of the tangential algorithm[21] (note that tangential curvature is synonymous with the instantaneous algorithm in the cited reference, which also incorrectly uses the term, "power" rather than curvature[22]).

Regression statistics are summarized in Table 3. For keratoconic eyes, ZKmax, CSpot_Axi, and CSpot_Tan were found to have a statistically significant negative relationship to both SP-A1 ($R^2 = 0.417$; $R^2 = 0.427$; $R^2 = 0.402$) and SP-HC ($R^2 = 0.192$; $R^2 = 0.201$; $R^2 = 0.200$) and a significantly positive relationship to both DA Ratio Max ($R^2 = 0.603$; $R^2 = 0.610$; $R^2 = 0.569$) and IIR ($R^2 = 0.728$; $R^2 = 0.746$; $R^2 = 0.694$), respectively. Stress–strain index demonstrated a statistically significant negative relationship to both CSpot_Axi and CSpot_Tan ($R^2 = 0.452$; $R^2 = 0.405$). Thus, corneal stiffness decreased by all biomechanical metrics as the severity of the disease, defined by cone curvature, increased in a continuous manner. Representative regression plots for SP-A1 and IIR vs. CSpot_Tan are given in Figure 3A, B.

For keratoconic eyes, Kmax_dist and CRad_Axi were found to have a significantly positive relationship to SP-A1 ($R^2 = 0.074$; $R^2 = 0.126$), no significant relationship to SP-HC, and a significantly negative relationship to both DA

Table 2. Summary of Biomechanical and Tomographic Parameters by Cone Location using Axial or Tangential Algorithms

Algorithm	Cone Location	Frequency	Kmax (D)	ZKmax (D)	CSpot_Axi (D)	CSpot_Tan (D)	Kmax_dist (mm)	CRad_Axi (mm)	CRad_Tan (mm)
Axial	Central	28 (42%)	59.09 ± 10.79	53.63 ± 9.03	56.66 ± 10.08	54.91 ± 9.30	0.877 ± 0.43	1.18 ± 0.29	0.71 ± 0.25
	Eccentric	39 (58%)	53.38 ± 6.20	49.89 ± 5.55	52.25 ± 5.92	52.94 ± 6.31	1.95 ± 0.608	1.97 ± 0.415	1.37 ± 0.414
P value	–	–	**P = 0.0159***	*P* = 0.0592	**P = 0.0449***	*P* = 0.3387	**P < 0.0001***	**P < 0.0001***	**P < 0.0001***
Tangential	Central	58 (87%)	56.63 ± 9.00	52.16 ± 7.50	54.88 ± 8.35	53.97 ± 7.79	1.29 ± 0.52	1.49± 0.37	0.95 ± 0.30
	Eccentric	9 (13%)	50.16 ± 4.98	46.88 ± 4.70	49.02 ± 4.57	52.45 ± 7.37	2.88 ± 0.55	2.66 ± 0.25	2.03 ± 0.35
P value	–	–	**P = 0.0398***	**P = 0.0451***	**P = 0.0443***	*P* = 0.5875	**P < 0.0001***	**P < 0.0001***	**P < 0.0001***

Algorithm	Cone Location	SP-A1 (mmHg/mm)	SP-HC (mmHg/mm)	SSI (Dimensionless)	DA Ratio (Dimensionless)	IIR (1/mm)	Age (yrs)	bIOP (mmHg)	CCT (μ)
Axial	Central	62.3 ± 25.7	7.71 ± 3.48	0.767 ± 0.173	6.62 ± 2.51	12.85 ± 4.39	32 ± 14	12.7 ± 3.1	483 ± 50
	Eccentric	73.7 ± 23.0	8.83 ± 3.57	0.922 ± 0.178	5.26 ± 0.78	10.18 ± 1.76	38 ± 12	13.4 ± 2.7	489 ± 49
P value	–	*P* = 0.0618	*P* = 0.2033	**P = 0.0007***	**P = 0.0096***	**P = 0.0045***	*P* = 0.1072	*P* = 0.3608	*P* = 0.2590
Tangential	Central	66.34± 24.1	7.97 ± 3.39	0.826 ± 0.174	6.02 ± 1.90	11.76 ± 3.36	35 ± 14	13.1 ± 2.9	479 ± 43
	Eccentric	85.8 ± 22.5	10.88 ± 3.73	1.056 ± 0.185	4.64 ± 0.61	8.31 ± 1.49	38 ± 7	13.2 ± 3.1	531 ± 63
P value	–	**P = 0.0260***	**P = 0.0209***	**P = 0.0005***	**P = 0.0001***	**P < 0.0001***	*P* = 0.5227	*P* = 0.8728	**P = 0.0059***

bIOP = biomechanically corrected intraocular pressure; CRad_Axi = distance from the corneal center to CSpot_Axi; CRad_Tan = distance from the corneal center to CSpot_Tan; CSpot_Axi = CLMI-derived steepest 2.0 mm diameter zone on the axial map; CSpot_Tan = CLMI-derived steepest 2.0 mm diameter zone on the tangential map; DA Ratio = deformation amplitude ratio at 2 mm; IIR = integrated inverse radius; Kmax = single point of maximum anterior axial curvature; Kmax_dist = distance between the corneal center and Kmax; SP-A1= stiffness parameter at first applanation; SP-HC = stiffness parameter at highest concavity; SSI = corneal stress–strain index; ZKmax = 2.0 mm diameter zone centered around Kmax.
*Indicates significant differences between central and eccentric cone locations.

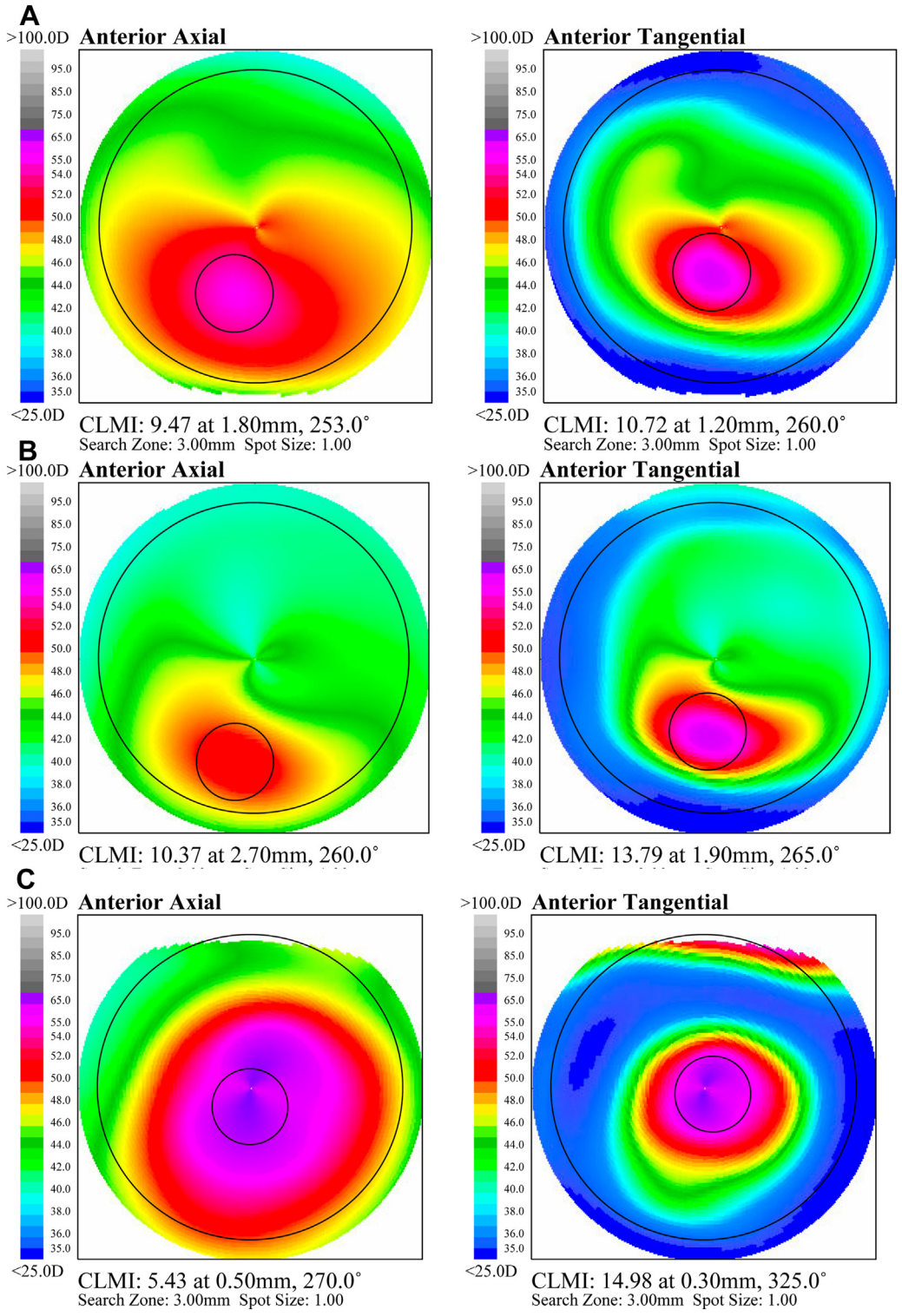

Figure 2. Pentacam data displayed with custom software showing **A,** Eccentric cone on axial map (CRad_Axi = 1.80 mm) and central cone on corresponding tangential map (CRad_Tan = 1.20 mm); **B,** Eccentric cone on both axial (CRad_Axi = 2.70 mm) and corresponding tangential map (CRad_Tan = 1.9); and **C,** Central cone on both axial (CRad_Axi= 0.5 mm) and corresponding tangential map (CRad_Tan = 0.3 mm). Note that the radial distance from the center is always larger on the axial map than the corresponding tangential map because the axial is a running average of the tangential radial distance with the difference between them becoming larger with distance from the center. Note also that the curvature pattern of the cone is the same on both algorithms, only much smaller and more central on the tangential maps. Note particularly the shape of the green isocurve on both map types. CLMI = Cone Location and Magnitude Index.

Table 3. Regression Statistics of Biomechanical vs. Tomographic Parameters

Y Parameter	X Parameter	*P* Value	R^2
SP-A1 (mmHg/mm)	ZKmax	**<0.0001***	0.4168
SP-HC (mmHg/mm)	ZKmax	**0.0004***	0.1922
DA Ratio (Dimensionless)	ZKmax	**<0.0001***	0.6031
IIR (1/mm)	ZKmax	**<0.0001***	0.7279
SP-A1 (mmHg/mm)	CSpot_Axi	**<0.0001***	0.4273
SP-HC (mmHg/mm)	CSpot_Axi	**0.0003***	0.2010
DA Ratio Max (Dimensionless)	CSpot_Axi	**<0.0001***	0.6102
IIR (1/mm)	CSpot_Axi	**<0.0001***	0.7457
SSI (Dimensionless)	CSpot_Axi	**<0.0001***	0.4516
SP-A1 (mmHg/mm)	CSpot_Tan	**<0.0001***	0.4020
SP-HC (mmHg/mm)	CSpot_Tan	**0.0003***	0.1999
DA Ratio Max (Dimensionless)	CSpot_Tan	**<0.0001***	0.5686
IIR (1/mm)	CSpot_Tan	**<0.0001***	0.6937
SSI (Dimensionless)	CSpot_Tan	**<0.0001***	0.4048
SP-A1 (mmHg/mm)	Kmax_dist	**0.0338***	0.0741
SP-HC (mmHg/mm)	Kmax_dist	0.2239	0.0250
DA Ratio Max (Dimensionless)	Kmax_dist	**0.0142***	0.0978
IIR (1/mm)	Kmax_dist	**0.0045***	0.1287
SP-A1 (mmHg/mm)	CRad_Axi	**0.005***	0.1262
SP-HC (mmHg/mm)	CRad_Axi	0.1135	0.0419
DA Ratio Max (Dimensionless)	CRad_Axi	**0.0002***	0.2063
IIR (1/mm)	CRad_Axi	**0.0001***	0.2342
SSI (Dimensionless)	CRad_Axi	**0.0002***	0.2061
SP-A1 (mmHg/mm)	CRad_Tan	0.2049	0.6002
	CCT	**<0.0001***	
SP-HC (mmHg/mm)	CRad_Tan	0.2664	0.4930
	CCT	**<0.0001***	
DA Ratio Max (Dimensionless)	CRad_Tan	**0.0151***	0.6804
	CCT	**<0.0001***	
IIR (1/mm)	CRad_Tan	**0.0002***	0.7472
	CCT	**<0.0001***	
SSI (Dimensionless)	CRad_Tan	**<0.0001***	0.4780
	CCT	**<0.0001***	

Note that the last 5 biomechanical metrics are from multiple regression analyses with CRad_Tan and CCT as independent variables and metric as the dependent variable.
CRad_Axi = distance from the corneal center to CSpot_Axi; CRad_Tan = distance from the corneal center to CSpot_Tan; CSpot_Axi = CLMI-derived steepest 2.0 mm diameter zone on the axial map; CSpot_Tan = CLMI-derived steepest 2.0 mm diameter zone on the tangential map; DA Ratio = deformation amplitude ratio at 2 mm; IIR = integrated inverse radius; Kmax = single point of maximum anterior axial curvature; Kmax_dist = distance between the corneal center and Kmax; SP-A1= stiffness parameter at first applanation; SP-HC = stiffness parameter at highest concavity; SSI = corneal stress–strain index; ZKmax = 2.0 mm diameter zone centered around Kmax.
*Indicates a significant relationship between Y and X parameters.

Ratio Max ($R^2 = 0.098$; $R^2 = 0.206$) and IIR ($R^2 = 0.129$; $R^2 = 0.234$), respectively. Kmax_dist showed a weaker, but still significant relationship to SP-A1 than CRad_Axi. Stress–strain index demonstrated a statistically significant positive relationship to CRad_Axi ($R^2 = 0.206$). Because there was a significant difference in CCT between central and eccentric cones using the tangential algorithm, multiple regression analyses were performed with CRad_Tan and CCT as independent variables and each biomechanical metric as the dependent variable. Neither SP-A1 nor SP-HC showed a significant relationship with CRad_Tan. However, DA Ratio Max, IIR, and SSI all showed a significant relationship to CRad_Tan consistent with greater stiffening corresponding to a greater distance from the center. Thus, most biomechanical metrics of corneal stiffness increased as the distance of the keratoconic cone from the center increased. Representative regression plots for SSI and IIR vs. CRad_Tan are given in Figure 4A, B.

Discussion

Our study supports the notion that KCN is driven by a focal structural deficit, rather than global weakening. Our results demonstrate that as the distance of the keratoconic cone from the central cornea increases, the stiffer the biomechanical response from the central cornea, analogous to the results obtained with the Ocular Response Analyzer.[23] The vastly unequal distribution of central (58) vs. eccentric (9) cones using the tangential algorithm likely led to the lack of a significant relationship between the SP-A1 metric and distance from the central cornea, because the relationship was significant when using the axial algorithm despite its averaging nature but having a more even distribution of subjects between groups. However, the premise of focal weakening when accurately locating the cone with the tangential algorithm is fully supported by the other 3 biomechanical metrics which demonstrated significant relationships. This model of focal weakening is also supported by Scarcelli et al,[11] who showed that the strength of the area outside of the cone was comparable to that of healthy corneal buttons. Thus, the cycle of biomechanical decompensation (Fig 5)[24] is dependent on focal weakness. The location of eccentric pathology may influence the ability to detect KCN with current techniques that rely on global biomechanical responses. Therefore, the use of tomography, in addition to biomechanical assessment, is important for the detection and screening of KCN patients until asymmetric biomechanical detection in a fast, reliable clinical device can be developed.[16,19]

In the analysis of tomographic parameters, we compared Zkmax which provides an average of the corneal curvature within the area around single-point Kmax. A number of recent studies have demonstrated the superiority of ZKmax over single-point Kmax in their reliability in detecting corneal changes after corneal cross-linking.[25–27] Others have demonstrated low levels of repeatability when utilizing single-point Kmax compared with zonal values and caution against using single-point values.[28,29] ZKmax has demonstrated greater repeatability between subsequent corneal scans because it is less prone to error than single-point Kmax.[30] In our own analysis, single-point Kmax was highly influenced by lid, tear film, and fixation, and varied widely between subsequent scans of the same eye. Therefore, we also advocate for the use of zonal measurements, rather than single-point measures. Furthermore, we demonstrate that CLMI-derived CSpot_Axi and CSpot_Tan may be located in different areas than ZKmax and more robustly pinpoint the location of the keratoconic cone than ZKmax, which is derived from the highly artifact-prone Kmax, as demonstrated in Figure 6, which also shows the thinnest location is closer to CSpot_Axi than Kmax.

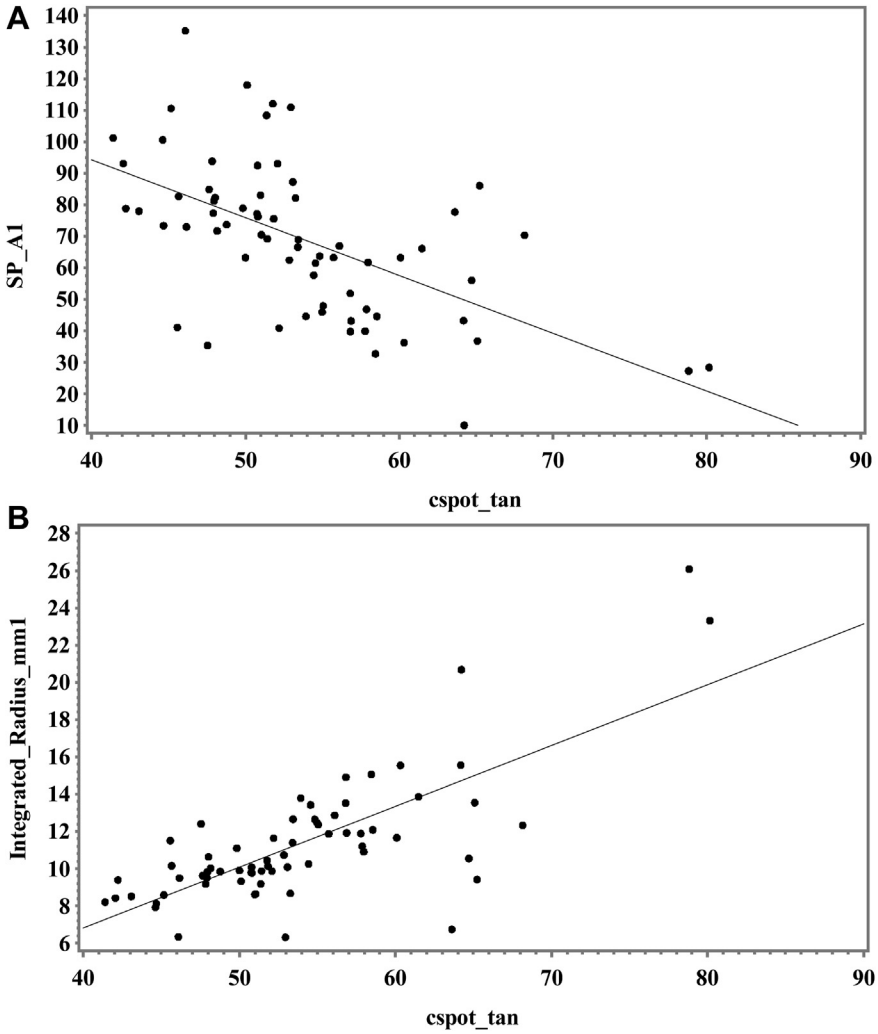

Figure 3. A, Stiffness parameter at first applanation (SP-A1) vs. magnitude of steepest 2 mm zone located by Cone Location and Magnitude Index on the tangential map (CSpot_Tan) of the keratoconic cone, showing decreasing stiffness with increasing severity; $P < 0.0001$; $R^2 = 0.4020$. **B,** Integrated inverse radius vs. magnitude of steepest 2 mm zone located by Cone Location and Magnitude Index on the tangential map (CSpot_Tan) of the keratoconic cone, showing increasing stiffness response (lower value) with increasing distance from the center; $P < 0.0001$; $R^2 = 0.6937$.

We chose to compare both axial and tangential maps in the evaluation of KCN as multiple studies have demonstrated substantial differences between the 2 algorithms.[23,31,32] Tangential maps are derived from the instantaneous radius of curvature and are therefore more sensitive to minute or subtle changes in corneal curvature.[31,32] Axial maps, however, use an algorithm that assumes corneal sphericity and is the mathematical average of the tangential map from center to periphery along each meridian.[23,31,32] Axial maps tend to "smooth" out the midperipheral cornea and cones on this display tend to be located more peripherally than their corresponding tangential displays.[23,28,29] By our own review, the vast majority of literature describing the location of the keratoconic cone relies on axial algorithms, which misrepresents the location of the greatest curvature zone due to its averaging nature. Therefore, the tangential algorithm more accurately locates the keratoconic cone than the axial, as illustrated in Figure 2. By evaluating the algorithms in the current study, we found that the majority of cones were located centrally within a 3 mm diameter from the corneal center using the tangential algorithm, rather than eccentrically as is normally assumed to be more prevalent. This finding contradicts the long-held belief that the keratoconic cone is located peripherally, primarily inferiorly or inferotemporally.[1,13,17] This finding is consistent with recent literature from Yuhas et al[23] that found that topographic analysis of tangential maps yielded a higher percentage of central cones than axial maps with an E300 Medmont topographer. Therefore, we recommend using tangential algorithms when characterizing the location of the keratoconic cone and conclude that the pathologic changes in KCN may be more central than previously reported.

Measures of corneal curvature are of particular importance when assessing the progression of KCN and the

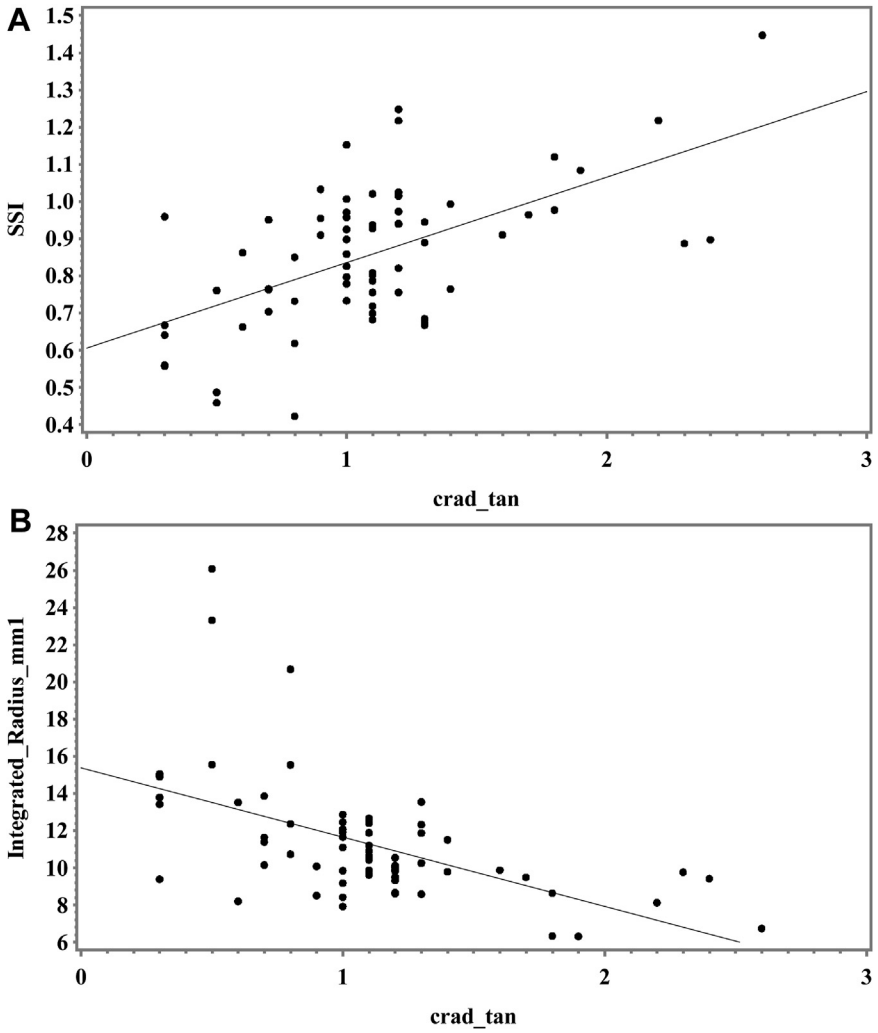

Figure 4. A, Stress–strain index (SSI) vs. distance from the corneal center to CSpot_Tan (CRad_Tan) of the keratoconic cone and central corneal thickness (CCT) in multiple regression, showing increasing stiffness with increasing distance from the center; CRad_Tan ($P < 0.0001$), CCT ($P < 0.0001$); $R^2 = 0.4780$. **B,** Integrated inverse radius vs. CRad_Tan of the keratoconic cone, showing increasing stiffness response (lower value) with increasing distance from the center; $P < 0.0001$; $R^2 = 0.2577$.

corneal response to cross-linking. Multiple recent meta-analyses have aptly concluded that corneal cross-linking successfully stabilizes corneal curvature.[33–36] However, these meta-analyses and the studies they contain rely on Kmax to determine corneal stability. The current study demonstrates that single-point Kmax on axial maps does not reliably locate the keratoconic cone. Therefore, to truly assess the progression of KCN and the corneal response to cross-linking, zonal measures of maximum curvature, particularly those derived from tangential maps, would be preferred. A comparison of the consequences of using Kmax vs. zonal Kmax in a randomized clinical trial comparing 2 crosslinking protocols was published in a letter that highlighted the dramatic difference in the number of failed cases with 3 times greater failures using single-point Kmax than zonal Kmax after 1 year. Using zonal Kmax altered the conclusions of this clinical trial and illustrated the robustness of using a zonal value instead of a single point.[37]

The detection of KCN and subclinical KCN is of the utmost importance in the preoperative screening of refractive surgery candidates. Keratoconus is an absolute contraindication to refractive surgery; however, cases of postsurgical ectasia continue to be reported.[2,6] Iatrogenic ectasia after refractive surgery has even been reported in patients with reassuring pachymetry, topography, tomography, and when using low levels of ablation.[38,39] A meta-analysis demonstrated that 27% of patients with iatrogenic ectasia had normal preoperative screening topography.[40] Thus, the preoperative detection of those at risk of developing ectasia is of paramount importance.

Many modalities, such as corneal thickness, corneal hysteresis, corneal-volume distributions, anterior corneal curvature, and posterior corneal elevation have been used to detect keratoconic changes.[3,16,41–43] However, each modality has its limitations. For example, topography is limited by corneal and tear film irregularities, while OCT interpolation may miss small areas of thickness variation.[44,45]

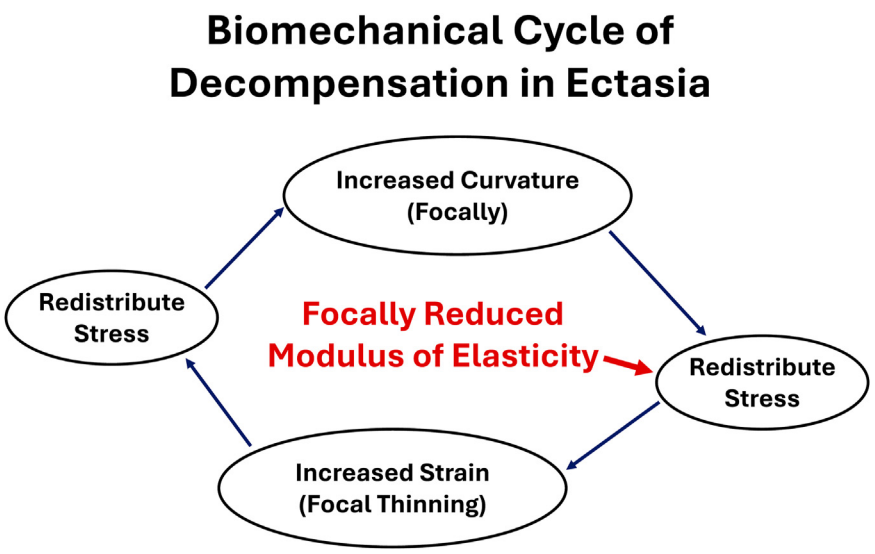

Figure 5. Biomechanical cycle of decompensation. Reprinted with permission from Roberts et al.[24]

Thus, many studies have concluded that individually, these methods have low diagnostic accuracy in detecting keratoconic patients, especially those with milder forms of KCN.[3,43,46,47] Therefore, combination assessments of tomography, pachymetry, and corneal biomechanics have become more widely used for the detection of KCN and at-risk corneas. Multiple studies have shown that these combinations have higher sensitivity and specificity in detecting both clinical and subclinical KCN than any of the methods alone.[16,19] Ambrósio et al[48] also recently demonstrated the use of artificial intelligence to analyze Pentacam tomography and Corvis ST biomechanical assessments to enhance ectasia detection than using biomechanics alone.

Recently, it has been proposed that many of the characteristic changes of KCN, such as thickness and corneal curvature, are precipitated by underlying biomechanical changes in the corneal stroma.[9,11,13] Biomechanical mediators such as inflammatory cytokines, extracellular matrix proteins, corneal enzymes, and even gene expression have been shown to be altered in keratoconic corneas.[49–53] These changes are then thought to lead to alterations in lamellar organization, keratocyte apoptosis, collagen expression, collagen cross-linking, and collagen degradation.[54–61] Further studies have shown that the altered collagen organization is confined only to the keratoconic cone, whereas the rest of the cornea is comparable with nonpathologic corneas.[62,63] Pahuja et al[63] provided evidence that altered gene expression and upregulation of inflammatory cytokines and metalloproteinases within the apex of the cone drive focal ultrastructural weakness in keratoconic corneas. Others have shown that the mechanical loss and thinning seen in KCN are focal in nature and isolated to the area of the keratoconic cone.[11,44] It has recently been reported that the stress distribution in KCN evolves over time from thickness driven with the thinnest point associated with greatest stress in normal corneas to curvature driven in KCN, where the area of greatest curvature near the thinnest point is associated with the lowest stress.[24]

Global indicators of biomechanical weakness, such as the Corvis biomechanical index, have been developed to characterize biomechanical corneal changes and have proven highly sensitive and specific for the detection of KCN.[14,15] However, biomechanical assessment of corneal response currently does not assess asymmetry. Owing to the focal nature of KCN, it is, therefore, necessary to factor spatial location into biomechanical assessments to enhance the detection of KCN at its earliest stages.[9] Various studies have shown that the detection of KCN is enhanced by the combination of tomography and biomechanics in creating indices such as the Tomographic and Biomechanical Index, which has proven to be more reliable in detecting ectasia than Corvis biomechanical index.[7,14,16,18] Ambrósio et al[48] demonstrated that combination assessments can be enhanced further through the utilization of artificial intelligence to detect ectatic patterns.

Limitations to our study include the use of a single center for data acquisition, which may limit the broader application of our results. Additionally, we acknowledge the use of custom CLMI software, which may not be widely accessible to the average clinician.

In conclusion, corneal stiffness decreases in KCN by all biomechanical metrics as the severity of the disease increases in a continuous manner defined by the curvature of the cone. Biomechanical metrics of central corneal stiffness increase as the distance of the keratoconic cone from the center increases, consistent with the focal nature of the biomechanical weakening in KCN. Zonal measures of KCN, especially those derived from CLMI, more robustly locate the keratoconic cone than single-point Kmax. Tangential, as opposed to axial, maps are preferred to be utilized in the management of KCN and demonstrate consistently more central pathology than previously

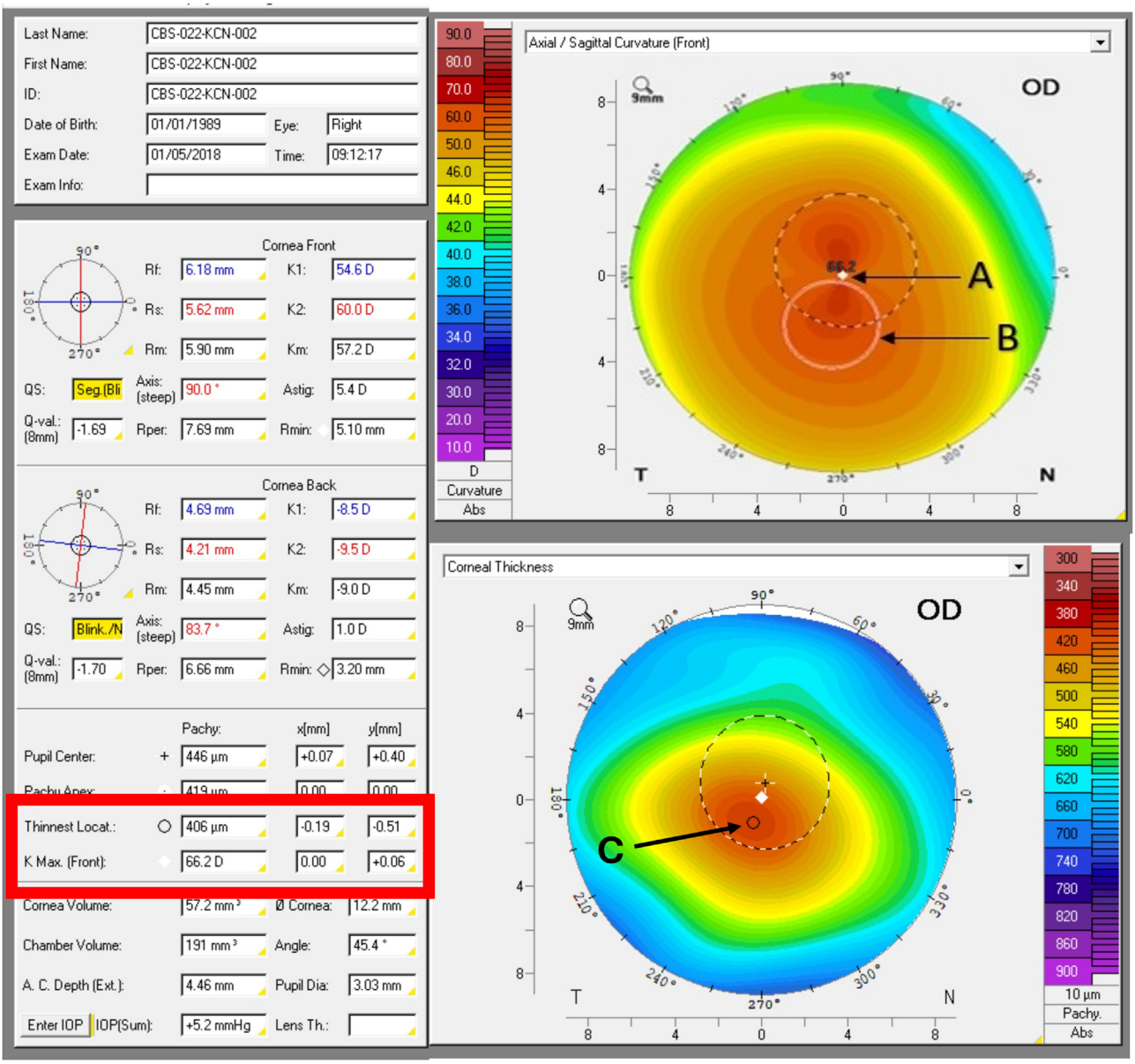

Figure 6. Spatial comparison of the single point of maximum anterior axial curvature (Kmax) and CSpot_Axi, showing that different locations are found when using single point (Kmax) and zonal value (CSpot_Axi). A = Kmax; B = CSpot_Axi. The corresponding pachymetry map, with C = thinnest location, demonstrates that the thinnest area and thinnest location are displaced from the center and closer to CSpot_Axi than Kmax.

reported. Further development is needed to produce a clinical biomechanical device that can assess the asymmetry of corneal biomechanics to better detect KCN at its earliest stages.

Acknowledgments

The authors appreciate the dedicated efforts of the Department of Ophthalmology and Visual Sciences Clinical Research Team for patient recruitment and diagnostic data collection.

Footnotes and Disclosures

Originally received: July 24, 2024.
Final revision: November 29, 2024.
Accepted: December 13, 2024.
Available online: December 20, 2024. Manuscript no. XOPS-D-24-00258R2.

[1] Ophthalmology & Visual Sciences, College of Medicine, The Ohio State University Wexner Medical Center, Columbus, Ohio.

[2] Biomedical Engineering, College of Engineering, The Ohio State University, Columbus, Ohio.

Disclosure(s):

All authors have completed and submitted the ICMJE disclosures form.

The author(s) have made the following disclosure(s):

C.J.R.: Consultant − Ziemer Ophthalmic Systems AG, Oculus Optikgeräte GmbH; Payment or honoraria for lectures, presentations, speakers bureaus, manuscript writing or educational events − Refractive Surgery Alliance Virtual Lecture; Support for attending meetings and/or travel − International Refractive Surgery Society, China (Sponsored by Society, May 2024), International Keratoconus Society, Muscat, Oman (Sponsored by Society, December 2023), European Society of Cataract and Refractive Surgery, Vienna, Austria (Sponsored by Society, September 2023), Visual and Physiological Optics, Antwerp, Belgium (Sponsored by Society, August 2023).

The other authors have no proprietary or commercial interest in any materials discussed in this article.

Supported in part by the grant National Institutes of Health/NEI R01 EY027399.

Support for Open Access publication was provided by The Ohio State University Department of Ophthalmology & Visual Sciences.

HUMAN SUBJECTS: Human subjects were included in this study. Institutional review board approval was obtained from The Ohio State University before the commencement of the study, which adhered to the Declaration of Helsinki. Informed consent was obtained from all participants before the initiation of data collection.

No animal subjects were used in this study.

Author Contributions:

Conception and design: Roberts

Data collection: Bruner

Analysis and interpretation: Bruner, Mahmoud, Roberts

Obtained funding: Roberts

Overall responsibility: Roberts

Abbreviations and Acronyms:
CCT = central corneal thickness; **CLMI** = Cone Location and Magnitude Index; **CRad_Axi** = radial distance of corneal center to CSpot_Axi; **CRad_Tan** = radial distance of corneal center to CSpot_Tan; **CSpot_Axi** = maximum curvature in 2 mm diameter zone on axial map located with CLMI; **CSpot_Tan** = maximum curvature in 2 mm diameter zone on tangential map located by CLMI; **DA Ratio** = deformation amplitude ratio at 2 mm; **IIR** = integrated inverse radius; **IOP** = intraocular pressure; **KCN** = keratoconus; **Kmax** = single point of maximum anterior axial curvature; **Kmax_dist** = distance between the corneal center and Kmax; **SP-A1** = stiffness parameter at first applanation; **SP-HC** = stiffness parameter at highest concavity; **SSI** = corneal stress−strain index; **ZKmax** = zonal value of maximum curvature in a 2 mm diameter circle around Kmax.

Keywords:
Biomechanics, Cornea, Corvis ST, Keratoconus, Tangential curvature.

Correspondence:
Cynthia J. Roberts, PhD, 915 Olentangy River Road, Columbus, OH 43212. E-mail: roberts.8@osu.edu.

References

1. Hashemi H, Heydarian S, Hooshmand E, et al. The prevalence and risk factors for keratoconus: a systematic review and meta-analysis. *Cornea*. 2020;39:263−270. https://doi.org/10.1097/ICO.0000000000002150.
2. Torres Netto EA, Al-Otaibi WM, Hafezi NL, et al. Prevalence of keratoconus in paediatric patients in Riyadh, Saudi Arabia. *Br J Ophthalmol*. 2018;102:1436−1441. https://doi.org/10.1136/bjophthalmol-2017-311391.
3. Fontes BM, Ambrósio Jr R, Jardim D, et al. Corneal biomechanical metrics and anterior segment parameters in mild keratoconus. *Ophthalmology*. 2010;117:673−679. https://doi.org/10.1016/j.ophtha.2009.09.023.
4. Nichols JJ, Steger-May K, Edrington TB, et al. The relation between disease asymmetry and severity in keratoconus. *Br J Ophthalmol*. 2004;88:788−791. https://doi.org/10.1136/bjo.2003.034520.
5. Davies PD, Lobascher D, Menon JA, et al. Immunological studies in keratoconus. *Trans Ophthalmol Soc U K (1962)*. 1976;96:173−178.
6. Mahmoud AM, Roberts CJ, Lembach RG, et al. CLMI: the cone location and magnitude index. *Cornea*. 2008;27:480−487. https://doi.org/10.1097/ICO.0b013e31816485d3.
7. Guo LL, Tian L, Cao K, et al. Comparison of the morphological and biomechanical characteristics of keratoconus, forme fruste keratoconus, and normal corneas. *Semin Ophthalmol*. 2021;36:671−678. https://doi.org/10.1080/08820538.2021.1896752.
8. Andreassen TT, Simonsen AH, Oxlund H. Biomechanical properties of keratoconus and normal corneas. *Exp Eye Res*. 1980;31:435−441. https://doi.org/10.1016/s0014-4835(80)80027-3.
9. Roberts CJ, Dupps Jr WJ. Biomechanics of corneal ectasia and biomechanical treatments. *J Cataract Refract Surg*. 2014;40:991−998. https://doi.org/10.1016/j.jcrs.2014.04.013.
10. Scarcelli G, Besner S, Pineda R, et al. In vivo biomechanical mapping of normal and keratoconus corneas. *JAMA Ophthalmol*. 2015;133:480−482. https://doi.org/10.1001/jamaophthalmol.2014.5641.
11. Scarcelli G, Besner S, Pineda R, Yun SH. Biomechanical characterization of keratoconus corneas ex vivo with Brillouin microscopy. *Invest Ophthalmol Vis Sci*. 2014;55:4490−4495. https://doi.org/10.1167/iovs.14-14450.
12. Meek KM, Tuft SJ, Huang Y, et al. Changes in collagen orientation and distribution in keratoconus corneas. *Invest Ophthalmol Vis Sci*. 2005;46:1948−1956. https://doi.org/10.1167/iovs.04-1253.
13. Gomes JAP, Tan D, Rapuano CJ, et al. Global consensus on keratoconus and ectatic diseases. *Cornea*. 2015;34:359−369. https://doi.org/10.1097/ICO.0000000000000408.
14. Vinciguerra R, Ambrósio Jr R, Elsheikh A, et al. Detection of keratoconus with a new biomechanical index. *J Refract Surg*. 2016;32:803−810. https://doi.org/10.3928/1081597X-20160629-01.
15. Ambrósio R Jr, Lopes BT, Faria-Correia F, et al. Integration of Scheimpflug-based corneal tomography and biomechanical assessments for enhancing ectasia detection. *J Refract Surg*. 2017;33:434−443. https://doi.org/10.3928/1081597X-20170426-02.
16. Kataria P, Padmanabhan P, Gopalakrishnan A, et al. Accuracy of Scheimpflug-derived corneal biomechanical and tomographic indices for detecting subclinical and mild keratectasia in a South Asian population. *J Cataract Refract Surg*. 2019;45:328−336. https://doi.org/10.1016/j.jcrs.2018.10.030.

17. Wu Y, Guo LL, Tian L, et al. Comparative analysis of the morphological and biomechanical properties of normal cornea and keratoconus at different stages. *Int Ophthalmol*. 2021;41: 3699−3711. https://doi.org/10.1007/s10792-021-01929-4.
18. Mahmoud AM, Nuñez MX, Blanco C, et al. Expanding the cone location and magnitude index to include corneal thickness and posterior surface information for the detection of keratoconus. *Am J Ophthalmol*. 2013;156:1102−1111. https://doi.org/10.1016/j.ajo.2013.07.018.
19. Koh S, Inoue R, Ambrósio Jr R, et al. Correlation between corneal biomechanical indices and the severity of keratoconus. *Cornea*. 2020;39:215−221. https://doi.org/10.1097/ICO.0000000000002129.
20. Roberts CJ, Mahmoud AM, Bons JP, et al. Introduction of two novel stiffness parameters and interpretation of air puff-induced biomechanical deformation parameters with a dynamic Scheimpflug analyzer. *J Refract Surg*. 2017;33: 266−273. https://doi.org/10.3928/1081597X-20161221-03.
21. Klein SA, Mandell RB. Axial and instantaneous power conversion in corneal topography. *Invest Ophthalmol Vis Sci*. 1995;36:2155−2159.
22. Roberts C. The accuracy of power maps to display curvature data in corneal topography systems. *Invest Ophth Vis Sci*. 1994;35:3525−3532.
23. Yuhas PT, Fortman MM, Mahmoud AM, Roberts CJ. Keratoconus cone location influences ocular biomechanical parameters measured by the Ocular Response Analyzer. *Eye Vis (Lond)*. 2024;11:2. https://doi.org/10.1186/s40662-023-00371-0.
24. Roberts CJ, Knoll KM, Mahmoud AM, et al. Corneal stress distribution evolves from thickness-driven in normal corneas to curvature-driven in keratoconus. *Ophthalmol Sci*. 2023;4: 100373.
25. Hashemi H, Amanzadeh K, Seyedian M, et al. Accelerated and standard corneal cross-linking protocols in patients with Down syndrome: a non-inferiority contralateral randomized trial. *Ophthalmol Ther*. 2020;9:1011−1021. https://doi.org/10.1007/s40123-020-00303-4.
26. Lytle G, Friedman M, Hersh P, Muller D. Use of zonal Km vs point Kmax for analysis of corneal cross-linking Pentacam topography. *Invest Ophthalmol Vis Sci*. 2013;54:5276.
27. Shah R, Lang P, Hafezi NL, et al. Comparison of outcomes between standard and accelerated corneal cross-linking protocols in patients with progressive keratoconus. *Invest Ophthalmol Vis Sci. 4400*. 2018;59:4400.
28. Steinwender G, Kollenc A, Shajari M, et al. Determining the center of a keratoconus: comparison of different tomographic parameters and impact of disease severity. *Front Med (Lausanne)*. 2022 Sep20;9:968318. https://doi.org/10.3389/fmed.2022.968318.
29. Sedaghat MR, Momeni-Moghaddam H, Azimi Khorasani A, et al. Comparison of keratoconus cone location of different topo/tomographical parameters. *Curr Eye Res*. 2021;46: 1666−1672. https://doi.org/10.1080/02713683.2021.1931343.
30. Asroui L, Mehanna CJ, Salloum A, et al. Repeatability of zone averages compared to single-point measurements of maximal curvature in keratconus. *Am J Ophthalmol*. 2021;221: 226−234. https://doi.org/10.1016/j.ajo.2020.08.011.
31. Rabinowitz YS. Tangential vs sagittal videokeratographs in the "early" detection of keratoconus. *Am J Ophthalmol*. 1996;122:887−889. https://doi.org/10.1016/s0002-9394(14)70388-5.
32. Gatinel D, Haouat M, Hoang-Xuan T. Etude des paramètres permettant la description mathématique de l'asphéricite cornéenne [A review of mathematical descriptors of corneal asphericity]. *J Fr Ophtalmol*. 2002;25:81−90.
33. McAnena L, Doyle F, O'Keefe M. Cross-linking in children with keratoconus: a systematic review and meta-analysis. *Acta Ophthalmol*. 2017;95:229−239. https://doi.org/10.1111/aos.13224.
34. Chunyu T, Xiujun P, Zhengjun F, et al. Corneal collagen cross-linking in keratoconus: a systematic review and meta-analysis. *Sci Rep*. 2014;4:5652. https://doi.org/10.1038/srep05652.
35. Kobashi H, Rong SS. Corneal collagen cross-linking for keratoconus: systematic review. *BioMed Res Int*. 2017;2017: 8145651. https://doi.org/10.1155/2017/8145651.
36. Ding L, Sun L, Zhou X. Network meta-analysis comparing efficacy and safety of different protocols of corneal cross-linking for the treatment of progressive keratoconus. *Graefes Arch Clin Exp Ophthalmol*. 2023;261:2743−2753. https://doi.org/10.1007/s00417-023-06026-z.
37. Hashemi H, Asgari S, Roberts CJ. Zonal Kmax is more reliable than single-point Kmax. *J Refract Surg*. 2021;37: 286−287. https://doi.org/10.3928/1081597X-20210204-02.
38. Klein SR, Epstein RJ, Randleman JB, Stulting RD. Corneal ectasia after laser in situ keratomileusis in patients without apparent preoperative risk factors. *Cornea*. 2006;25:388−403. https://doi.org/10.1097/01.ico.0000222479.68242.77.
39. Ambrósio R Jr, Dawson DG, Salomão M, et al. Corneal ectasia after LASIK despite low preoperative risk: tomographic and biomechanical findings in the unoperated, stable, fellow eye. *J Refract Surg*. 2010;26:906−911. https://doi.org/10.3928/1081597X-20100428-02.
40. Randleman JB, Woodward M, Lynn MJ, Stulting RD. Risk assessment for ectasia after corneal refractive surgery. *Ophthalmology*. 2008;115:37−50. https://doi.org/10.1016/j.ophtha.2007.03.073.
41. Mandell RB, Polse KA. Keratoconus: spatial variation of corneal thickness as a diagnostic test. *Arch Ophthalmol*. 1969;82:182−188. https://doi.org/10.1001/archopht.1969.00990020184006.
42. Ambrósio Jr R, Alonso RS, Luz A, Coca Velarde LG. Corneal-thickness spatial profile and corneal-volume distribution: tomographic indices to detect keratoconus. *J Cataract Refract Surg*. 2006;32:1851−1859. https://doi.org/10.1016/j.jcrs.2006.06.025.
43. Shah S, Laiquzzaman M, Bhojwani R, et al. Assessment of the biomechanical properties of the cornea with the ocular response analyzer in normal and keratoconic eyes. *Invest Ophthalmol Vis Sci*. 2007;48:3026−3031. https://doi.org/10.1167/iovs.04-0694.
44. Li Y, Meisler DM, Tang M, et al. Keratoconus diagnosis with optical coherence tomography pachymetry mapping. *Ophthalmology*. 2008;115:2159−2166. https://doi.org/10.1016/j.ophtha.2008.08.004.
45. Li Y, Shekhar R, Huang D. Corneal pachymetry mapping with high-speed optical coherence tomography. *Ophthalmology*. 2006;113: 792−799.e2. https://doi.org/10.1016/j.ophtha.2006.01.048.
46. Saad A, Lteif Y, Azan E, Gatinel D. Biomechanical properties of keratoconus suspect eyes. *Invest Ophthalmol Vis Sci*. 2010;51:2912−2916. https://doi.org/10.1167/iovs.09-4304.
47. Jonsson M, Behndig A. Pachymetric evaluation prior to laser in situ keratomileusis. *J Cataract Refract Surg*. 2005;31: 701−706. https://doi.org/10.1016/j.jcrs.2005.02.028.
48. Ambrósio R Jr, Machado AP, Leão E, et al. Optimized artificial intelligence for enhanced ectasia detection using Scheimpflug-based corneal tomography and biomechanical

data. *Am J Ophthalmol*. 2023;251:126−142. https://doi.org/10.1016/j.ajo.2022.12.016.
49. Shetty R, D'Souza S, Khamar P, et al. Biochemical markers and alterations in keratoconus. Asia Pac. *J Ophthalmol (Phila)*. 2020;9:533−540. https://doi.org/10.1097/APO.0000000000000332.
50. Matthews FJ, Cook SD, Majid MA, et al. Changes in the balance of the tissue inhibitor of matrix metalloproteinases (TIMPs)-1 and -3 may promote keratocyte apoptosis in keratoconus. *Exp Eye Res*. 2007;84:1125−1134. https://doi.org/10.1016/j.exer.2007.02.013.
51. Wisse RP, Kuiper JJ, Gans R, et al. Cytokine expression in keratoconus and its corneal microenvironment: a systematic review. *Ocul Surf*. 2015;13:272−283. https://doi.org/10.1016/j.jtos.2015.04.006.
52. Ghosh A, Zhou L, Ghosh A, et al. Proteomic and gene expression patterns of keratoconus. *Indian J Ophthalmol*. 2013;61:389−391. https://doi.org/10.4103/0301-4738.116056.
53. Kenney MC, Nesburn AB, Burgeson RE, et al. Abnormalities of the extracellular matrix in keratoconus corneas. *Cornea*. 1997;16:345−351. https://doi.org/10.1097/00003226-199705000-00016.
54. Blackburn BJ, Jenkins MW, Rollins AM, Dupps WJ. A review of structural and biomechanical changes in the cornea in aging, disease, and photochemical crosslinking. *Front Bioeng Biotechnol*. 2019;7:66. https://doi.org/10.3389/fbioe.2019.00066.
55. White TL, Lewis PN, Young RD, et al. Elastic microfibril distribution in the cornea: differences between normal and keratoconic stroma. *Exp Eye Res*. 2017;159:40−48. https://doi.org/10.1016/j.exer.2017.03.002.
56. Kim WJ, Rabinowitz YS, Meisler DM, Wilson SE. Keratocyte apoptosis associated with keratoconus. *Exp Eye Res*. 1999;69:475−481. https://doi.org/10.1006/exer.1999.0719.
57. Shetty R, Sathyanarayanamoorthy A, Ramachandra RA, et al. Attenuation of lysyl oxidase and collagen gene expression in keratoconus patient corneal epithelium corresponds to disease severity. *Mol Vis*. 2015;21:12−25.
58. Chaerkady R, Shao H, Scott SG, et al. The keratoconus corneal proteome: loss of epithelial integrity and stromal degeneration. *J Proteomics*. 2013;87:122−131. https://doi.org/10.1016/j.jprot.2013.05.023.
59. Cheng EL, Maruyama I, SundarRaj N, et al. Expression of type XII collagen and hemidesmosome-associated proteins in keratoconus corneas. *Curr Eye Res*. 2001;22:333−340. https://doi.org/10.1076/ceyr.22.5.333.5491.
60. Takaoka A, Babar N, Hogan J, et al. An evaluation of lysyl oxidase-derived cross-linking in keratoconus by liquid chromatography/mass spectrometry. *Invest Ophthalmol Vis Sci*. 2016;57:126−136. https://doi.org/10.1167/iovs.15-18105.
61. Foster CS, Yamamoto GK. Ocular rigidity in keratoconus. *Am J Ophthalmol*. 1978;86:802−806. https://doi.org/10.1016/0002-9394(78)90125-3.
62. Radner W, Zehetmayer M, Skorpik C, Mallinger R. Altered organization of collagen in the apex of keratoconus corneas. *Ophthal Res*. 1998;30:327−332. https://doi.org/10.1159/000055492.
63. Pahuja N, Kumar NR, Shroff R, et al. Differential molecular expression of extracellular matrix and inflammatory genes at the corneal cone apex drives focal weakening in keratoconus. *Invest Ophthalmol Vis Sci*. 2016;57:5372−5382. https://doi.org/10.1167/iovs.16-19677.